JOURNAL OF COMPUTATIONAL PHYSICS 27, 272–283 (1978)

High-Resolution and Efficient Calculation of Photoelectric Spectra of Crystals

R. CAR, G. CIUCCI, AND L. QUARTAPELLE

Istituto di Fisica del Politecnico di Milano, Italy

Received May 12, 1977; revised July 26, 1977

The Dalton–Gilat method for calculating photoelectric spectra of crystalline solids is considered, improved, and implemented. Spectral integration is performed by means of linear analytic approximation which assures high resolution, accuracy, and efficiency. The interest of the method is not limited to problems of solid state physics since it also provides a general numerical algorithm for the approximate computation of three-dimensional line integrals of rapidly varying functions.

1. INTRODUCTION

The photoelectric spectra of solids describe the energy distribution of electrons emitted from crystals by electromagnetic radiation of given frequency. The measured energy distribution curves can be related to crystal electron states in a more or less direct way depending on the various physical assumptions which prove adequate to the considered situation.

A widely applicable and frequently used model is the so-called direct transition model which assumes that the photoelectric transitions occur between electron states with the same reduced quasi-momentum. In this model the spectral intensity depends only on the electron states belonging to one-dimensional manifolds of the Brillouin zone so that the calculation of photoelectric spectra from band structure amounts to locating and computing line integrals in the reciprocal space of **k**-vectors. (The opposite model based on indirect transitions leads to a much simpler relation and it will not be considered here.) Analogous problems of line integral computation are encountered in the determination of the de Haas–van Alphen areas and cyclotron masses, the lines now lying on the Fermi surface of the metal.

A traditional technique used for this kind of calculations is the root-sampling method [1–3]. A large number of **k**-points are generated inside the Brillouin zone and at these points the electron energies are computed by direct spectralization of the Hamiltonian or by suitable interpolations over a coarser mesh [1]. Then the eigenvalues are selected and grouped to provide a histogram representation of the spectrum.

0021-9991/78/0272–0272$02.00/0

An entirely different method has been proposed by Dalton and Gilat [4] by generalizing to line integrals the Gilat–Raubenheimer zonal integration method for surface integrals. This method relies on analytical integration inside small rectangular prisms where the integration curve is approximated by a straight line. Although theoretical spectra obtained by means of special adaptations of this method to simple cases of high symmetry crystals had been previously reported [5–7], only [4] gives the method a general form allowing a broader class of applications. Nevertheless, and in spite of its substantial advantages, the Dalton–Gilat algorithm has never been implemented, probably because of some complications apparent in the presentation, apart from some misprints in the analytical relations.

In this paper an improved version of the Dalton–Gilat algorithm is presented. The proposed improvement is such that the transition probability of photoexcitation is taken into account within linear approximation so as to reproduce fine details of the spectrum with lower numerical distortion, at a fixed computational effort. Therefore this modification to the original Dalton–Gilat algorithm parallels the analogous one proposed by Gilat and Kam [9] to the Gilat–Raubenheimer method for surface integrals [8].

The presence of the linear term accounting for rapid variations of the integrand function inside the prism and the shape of rectangular prisms matching many different integration domains make this algorithm a general numerical method to compute approximate line integrals in a three-dimensional space. As a matter of fact, to disregard higher order terms may cause convergence problems in regions where the integrand has pathological behavior. This may happen, for instance, to line integrals in unbounded domains when the algorithm is used after mapping the integration domain into a bounded one. With this concern in mind the algorithm can also be applied to problems different from those of solid state physics for which it had been originally developed.

The paper also presents an application of the algorithm to the calculation of the energy distribution spectra of photoexcited electrons in the nearly-free-electron model. A semiquantitative assessment of the accuracy and resolution of the method is attempted by comparing approximate and exact values of the spectra.

The exposition is divided as follows. Section 2 contains the description of the integration algorithm and all the relevant analytical relations required for its direct implementation. Section 3 discusses the computational performances of the method in connection with the numerical results obtained for the nearly-free-electron model. The analytical solution of the initial-energy distribution of photoexcited electrons in the first interband transition of the model is derived in the Appendix.

2. The Method

The widely used three-step model [10, 12] envisages the photoemission process as consisting of three independent steps: optical excitation via direct (vertical) interband transitions in the bulk of the crystal, electron transport to the surface, and electron

escape across the surface. The internal distribution $N(E, \omega)$ of final energy E of the electrons excited by electromagnetic radiation of fixed frequency ω is given by

$$N(E, \omega) = C\Sigma_{i,f} \int_{BZ} d^3k \mid p_{if}(\mathbf{k})|^2 \times f^0(E_i(\mathbf{k})) \times [1 - f^0(E_f(\mathbf{k}))] \times \delta(\omega - E_f(\mathbf{k}) + E_i(\mathbf{k})) \times \delta(E - E_f(\mathbf{k})) \tag{1}$$

where $p_{if}(\mathbf{k})$ is the matrix element of the transition between the initial state i and the final state f, $f^0(E)$ is the Fermi–Dirac distribution function, and C is some normalization constant.

Electron transport and escape are usually taken into account according to phenomenological models [10] which lead to spectral relations differing from (1) only in that a more involved integrand function is implied. Without any loss of generality it is assumed hereafter that all the integrand functions are lumped together with the term $\mid p_{if}(\mathbf{k})|^2$.

Physically the first delta function in relation (1) selects the set of electron states satisfying energy conservation in optical excitation and lying on a $\mathbf{k}$-space surface, the so-called optical energy shell [12]. The second delta selects from this set of states those with the correct final energy E, so defining a curve $L(E, \omega)$ in the $\mathbf{k}$-space [12]. In fact the integral (1) can be transformed into the line integral

$$N(E, \omega) = C\Sigma_{i,f} \int_{L(E,\omega)} \frac{\mid p_{if}(\mathbf{k})|^2 \, dL}{\mid \nabla E_{fi}(\mathbf{k}) \times \nabla E_f(\mathbf{k})|}, \tag{2}$$

where $E_{fi} = E_f - E_i$.

The integral will be computed by dividing the integration domain into small rectangular prisms of sides $2p_1$, $2p_2$, and $2p_3$ and then, within each prism, replacing the functions $E_{fi}(\mathbf{k})$, $E_f(\mathbf{k})$, and $\mid p_{if}(\mathbf{k})|^2$ by the first two terms in their power series expansion about the center $\mathbf{k}_0$ of the prism [4]. One is led to compute integrals of the type

$$I(A_0, B_0) = \frac{1}{\mid \mathbf{A} \times \mathbf{B} \mid} \int_{\Delta L(A_0, B_0)} (F_0 + \mathbf{F} \cdot \mathbf{q}) \, dL, \tag{3}$$

where by definition $\mathbf{q} = \mathbf{k} - \mathbf{k}_0$,

$$F_0 = \mid p_{if}(\mathbf{k}_0)|^2, \qquad \mathbf{F} = \nabla \mid p_{if}(\mathbf{k}_0)|^2,$$
$$A_0 = \omega - E_{fi}(\mathbf{k}_0), \qquad \mathbf{A} = \nabla E_{fi}(\mathbf{k}_0),$$
$$B_0 = E - E_f(\mathbf{k}_0), \qquad \mathbf{B} = \nabla E_f(\mathbf{k}_0),$$

and $\Delta L(A_0, B_0)$ is the length of the portion of the line of intersection between the planes $\mathbf{A} \cdot \mathbf{q} = A_0$ and $\mathbf{B} \cdot \mathbf{q} = B_0$ which lies within the prism. Integral (3) differs from the analogous relation in [4] in that the linear term is retained. The explicit relations for the analytical evaluation of (3) are now derived by rephrasing the geometrical arguments of Dalton and Gilat so as to obtain simpler analytical relations.

Introducing the spatial homothety of ratio $p_1 p_2 p_3$ and using the same symbol as before for the scaled vectors we arrive at

$$I = p_1 p_2 p_3 \frac{1}{|\mathbf{A} \times \mathbf{B}|} \int_{\Delta L} (F_0 + \mathbf{F} \cdot \mathbf{q})\, dL = p_1 p_2 p_3 \frac{(F_0 + \mathbf{F} \cdot \mathbf{Q})\, \Delta L}{|\mathbf{A} \times \mathbf{B}|}, \tag{4}$$

where ΔL is now the scaled length of the line portion inside the cube and $\mathbf{Q}$ is the position of the center of this straight segment with respect to the cube center.

Let $\mathbf{C} = \mathbf{A} \times \mathbf{B}$ be the vector in the direction of the line ΔL and $\mathbf{c} = \mathbf{C}/C$ the corresponding unit vector. Let the directions of q_i be chosen so that $c_3 \geqslant c_2 \geqslant c_1 \geqslant 0$. A new Cartesian coordinate system (u_1, u_2, u_3) is introduced such that $\hat{\mathbf{u}}_3 = \mathbf{c}$ and $\hat{\mathbf{u}}_2 \cdot \hat{\mathbf{q}}_1 = 0$, where $\hat{\mathbf{q}}_1$, $\hat{\mathbf{u}}_2$, and $\hat{\mathbf{u}}_3$ are axis unit vectors, by means of the transformation matrix

$$T = \begin{bmatrix} s & -c_1 c_2/s & -c_1 c_3/s \\ 0 & c_3/s & -c_2/s \\ c_1 & c_2 & c_3 \end{bmatrix},$$

where $s = (1 - c_1^2)^{1/2}$. Then the coordinates U_1 and U_2 of the line ΔL in the plane (u_1, u_2) are given by the linear system

$$\begin{aligned} a_1 U_1 + (\mathbf{a} \times \mathbf{c})_1\, U_2 &= s a_0, \\ b_1 U_1 + (\mathbf{b} \times \mathbf{c})_1\, U_2 &= s b_0, \end{aligned} \tag{5}$$

where $a_i = A_i/A$ and $b_i = B_i/B$, with $i = 0, 1, 2, 3$.

If $U_2 < 0$ let the signs of U_1 and U_2, and of all the components of the vector $T\mathbf{F}$, be changed (the rotation is chosen in place of the reflection to reduce to a minimum the number of analytical relations).

In the general case $c_3 > c_2 > c_1 > 0$ it can be shown that five distinct domains of the half-plane $(u_1, u_2 \geqslant 0)$ given in Table I correspond to intersections of the line ΔL with different couples of cube faces. The values of the length ΔL and the center coordinate U_3' of the portion of the line inside the cube can be calculated for each distinct domain and they are listed in Table I. The degenerate case $c_3 > c_2 > c_1 = 0$ $(1 = c_3 > c_2 = c_1 = 0)$ gives rise to only two (one) distinct domains (domain) and can be dealt with by means of the same relations of Table I restricted to domains I and II (I). System (5) will be solved by factorizing its matrix once and then performing substitutions for all distinct pairs (a_0, b_0).

The greatest numerical errors in the computation of the integral (2) are made at critical points of the $\mathbf{k}$-space, i.e., points where $|\nabla E_{fi}(\mathbf{k}) \times \nabla E_f(\mathbf{k})| = 0$. The vanishing of the vector product can result from the vanishing of either of the vectors or from the coincidence of their directions. The latter circumstance is the most frequent and gives rise to singular spectral behaviors of three kinds: left and right square discontinuities and logarithmically infinite peaks [12], which correspond to the three types of critical points of a function periodic in two dimensions, i.e., lower and upper extrema and saddle points, respectively [13].

TABLE I

Analytical Relations for the Length ΔL and the Center Coordinate U_3' of the Straight Segment inside a Cube[a]

	U_1	U_2	ΔL	U_3'
I	$[-sc_{1/3}^{-} - c_{12/3}U_2\,,\ +sc_{1/3}^{-} - c_{12/3}U_2]$	$[0,\ (c_3 - c_2)/s]$	$2c_{/3}$	$(c_1U_1 + c_{2/3}U_2)/s$
II	$[-sc_{1/3}^{-} - c_{12/3}U_2\,,\ +sc_{1/2}^{-} + c_{13/2}U_2]$	$[(c_3 - c_2)/s,\ (c_3 + c_2)/s]$	$c_{/23}s((c_3 + c_2)/s - U_2)$	$(c_1U_1 + \frac{1}{2}(c_{2/3} - c_{3/2})U_2 + \frac{1}{2}(c_{/2} - c_{/3})s^2)/s$
III	$[-sc_{1/2}^{+} + c_{13/2}U_2\,,\ -sc_{1/3}^{-} - c_{12/3}U_2]$	$[(c_3 - c_2)/s,\ (c_3 + c_2)/s]$	$c_{/1}(sc_{1/2}^{+} + U_1 - c_{13/2}U_2)/s$	$c_{/1}(+\bar{s}U_1 - \frac{1}{2}c_{13/2}U_2 - \frac{1}{2}sc_{1/2}^{-})/s$
IV_a	$[-sc_{1/3}^{+} - c_{12/3}U_2\,,\ -sc_{1/3}^{-} - c_{12/3}U_2]$	$[0,\ (c_3 - c_2)/s]$	$c_{/1}(sc_{1/3}^{+} + U_1 + c_{12/3}U_2)/s$	$c_{/1}(+\bar{s}U_1 + \frac{1}{2}c_{12/3}U_2 - \frac{1}{2}sc_{1/3}^{-})/s$
IV_b	$[+sc_{1/3}^{-} - c_{12/3}U_2\,,\ +sc_{1/3}^{+} - c_{12/3}U_2]$	$[0,\ c_{2/13}(-sc_{1/2}^{-} + U_1)]$	$c_{/1}(sc_{1/3}^{+} - U_1 - c_{12/3}U_2)/s$	$c_{/1}(+\bar{s}U_1 + \frac{1}{2}c_{12/3}U_2 + \frac{1}{2}sc_{1/3}^{-})/s$

[a] ($c_{ij} = c_ic_j$, $c_{i/j} = c_i/c_j$, $c_{/i} = 1/c_i$, etc., $c^+ = 1 + c$, $c^- = 1 - c$, $s = (1 - c_1^2)^{1/2}$, and $\bar{s} = \frac{1}{2} - s^2$).

The spectral integration of contributions coming from these critical regions is necessarily inaccurate, no matter what the method, and linear analytic methods are no exception [14]. However, as emphasized in [15], analytic integration is no less accurate than other methods even in these critical regions. Anyway, the use of a mesh shifted with respect to the coordinate axis will reduce the error due to most critical points since for symmetry reasons it is highly probable their location is on the surfaces of the Brillouin zone. Information about the critical points and critical lines can be obtained by the two-dimensional analysis over the zone boundaries [12] which is complementary to three-dimensional calculations through the bulk of the zone.

3. Application to the Nearly-Free-Electron Model

To investigate the resolution and accuracy of the algorithm the nearly-free-electron model has been chosen since it is possible to derive analytically its energy distributions of photoexcited electrons over the full range of photon energy (see the Appendix). Furthermore these spectra display the singular behavior of physical spectra and therefore represent a good test for the integration method. The first band has been assumed entirely filled and the integration domain shown in Fig. 1 has been chosen so as to compare directly the exact and approximate values.

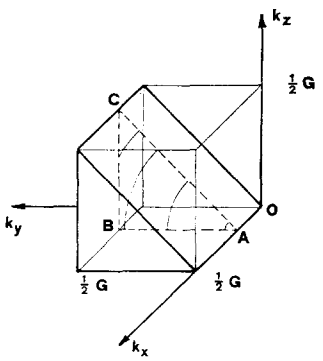

Fig. 1. Integration domain of the k-space for the nearly-free-electron model.

Figure 2 displayes in a three-dimensional plot all spectra, whose photon energy ranges from the lowest value for transitions at the band gap, to the highest value for transitions involving states at the bottom of the valence band. The first dimensionless Fourier component $V_G/(\frac{1}{2}G)^2$ of the periodic potential is equal to 0.3 and a constant dipole matrix element is assumed.

The spectrum $N(E, \omega)$ for a fixed ω has a left square edge discontinuity due to the critical point A shown in Fig. 1 where the electron energy surface has a minimum over the optical energy shell, the plane ABC in Fig. 1. On the other hand, the square

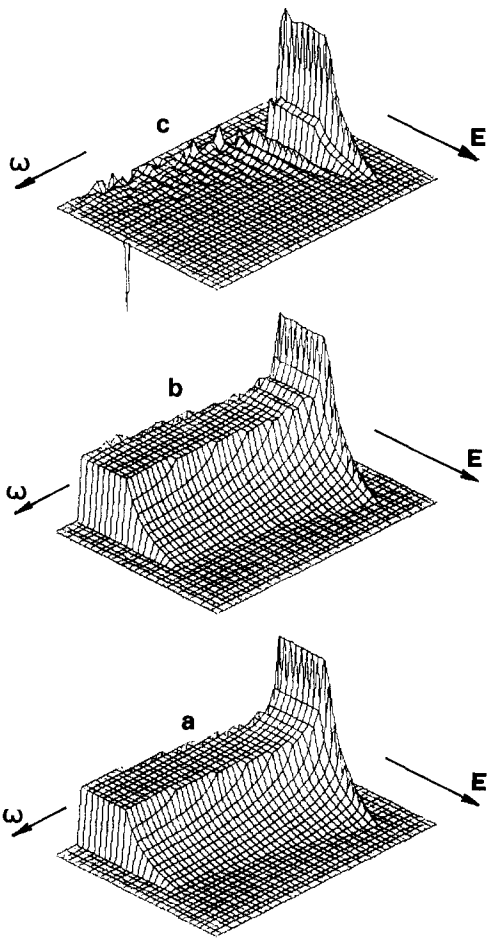

FIG. 2. Initial-energy distributions $N(E, \omega)$ of photoexcited electrons in the nearly-free-electron model. $V_G/(\frac{1}{2}G)^2 = 0.3$ and the transition probability is constant: (a) exact, (b) calculated, (c) error (scale $\times$ 10).

edge discontinuity displayed for a fixed E and varying ω, can be explained as resulting from the contribution of an entire curve where the optical energy shell has an extended maximum with nonzero derivative normal to the curve. The asymptotic behavior at minimum photon energy is due to the vanishing of ∇E_{fi} for optical transitions at the band gap (note that this structure in the internal distribution will be removed when passing to photoemission spectra owing to the cutoff imposed by the work function). Finally, the two lines where the slope of the spectrum changes are a consequence of the cutoff caused by the shape of the integration domain (see points B and C in Fig. 1). It is noticed that the rectangular box shape of the spectrum at fixed ω and the intensity dependence on ω are consistent with the results obtained in [2] for the nearly-free-electron model of a metal.

Numerical tests have been performed by means of this model with the additional feature of a transition probability $|p_{if}(\mathbf{k})|^2$ varying as $(k_y/\frac{1}{2}G)^m$, with m an integer. Components of ∇E_{fi} have received a slight perturbation, smaller than truncation errors, to obtain performance estimates meaningful also for nondegenerate situations.

Figures 2 and 3 display the exact spectra, the calculated spectra, and the numerical error, for constant and varying dipoles, respectively. The approximate calculation is performed with 4000 small prisms in the integration domain and the number of energy values considered is $n_E = 30$ and $n_\omega = 45$, which corresponds to resolutions of 3×10^{-2} and 2×10^{-2} respectively. In both cases an average accuracy of $\sim 10^{-2}$ is obtained by a very limited computational effort of $\sim$10 sec (UNIVAC 1108) for the calculation of $\sim$1000 distinct line integrals. The error plots clearly show that the

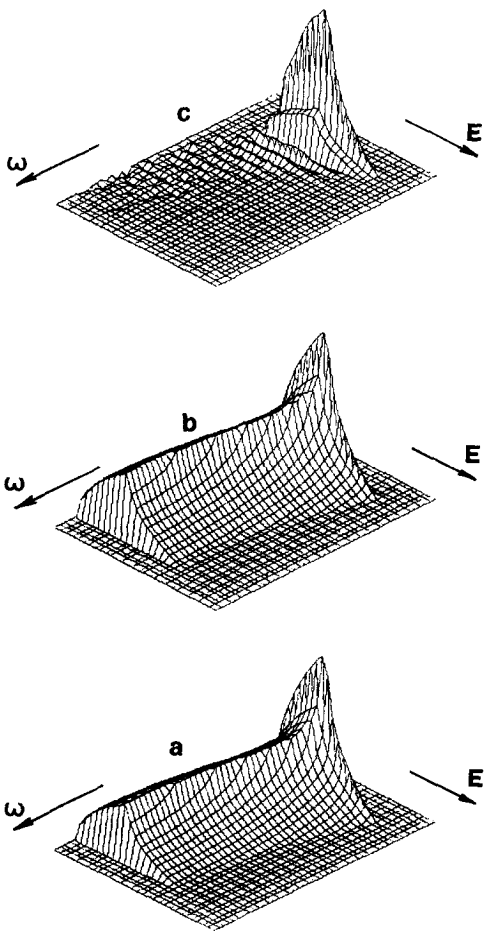

FIG. 3. Initial-energy distributions $N(E, \omega)$ of photoexcited electrons in the nearly-free-electron model. $V_G/(\frac{1}{2}G)^2 = 0.3$ and the transition probability varies as $(k_y/\frac{1}{2}G)$: (a) exact, (b) calculated, (c) error (scale $\times 10$).

greatest numerical distortions take place near the asymptote and the square edge discontinuity.

The nearly-free-electron model also allows us to show the advantage of using the improved algorithm in place of the Dalton–Gilat algorithm, as shown in Fig. 4 where a single spectrum with a dipole varying as $(k_y/\frac{1}{2}G)^5$ is given together with the curves of the numerical error of the two algorithms. The comparison between the errors shows that the improved algorithm achieves a sensibly higher accuracy although its local error can be larger somewhere. The calculation of this single spectrum with $n_E = 100$ and 8000 small prisms requires $\sim$0.25 sec and an average accuracy of 2×10^{-3} is obtained.

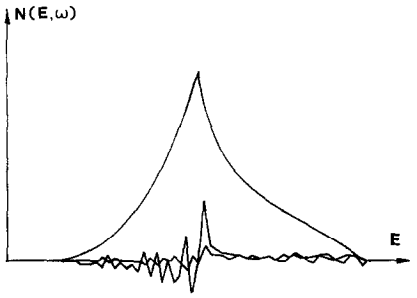

FIG. 4. Initial-energy distribution $N(E, \omega)$ for $\omega/(\frac{1}{2}G)^2 = 2.5$ of photoexcited electrons in the nearly-free-electron model. $V_G/(\frac{1}{2}G)^2 = 0.3$ and the transition probability varies as $(k_y/\frac{1}{2}G)^5$. The lower curves show the numerical error (scale $\times$ 10) of the original and of the improved integration algorithm.

To have some figures meaningful for physical calculations the computed photoelectric spectrum at $\omega = 10.5$ eV of the crystalline compound SnTe [16] is reported in Fig. 5. An accuracy and a resolution of 10^{-2} are obtained by means of $\sim$10,000

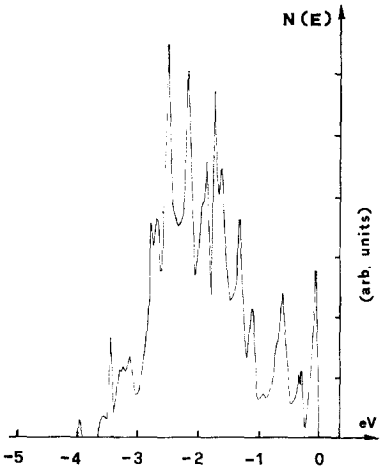

FIGURE 5

small prisms quadratically interpolated [17] over the coarser mesh of 185 computed points. The calculation involves 65 interband transitions and requires ~20 sec of computation, which compares favorably with the ~30 min required by the root-sampling method to achieve comparable resolution and accuracy.

4. Conclusion

The method for computing photoelectric spectra of crystals here presented fully exploits all the advantages of linear analytic methods for spectral integration. The algorithm has proved to be noticeably more accurate than its direct ancestor [4] without requiring a substantial increase in the computational effort. These distinctive features make the algorithm particularly suited to accomplish detailed theoretical analysis of presently relevant photoelectric measurements performed by means of the continuous spectrum of synchrotron radiation. Moreover it can also conveniently be applied in carrying out extensive studies of the reciprocal space origin of the photoelectric structures as required when investigating the consequences of a theoretical model of band structure.

If computational convenience severely limits the number of **k**-points where the Hamiltonian can be spectralized, this linear analytic method lends itself to being directly coupled to the quadratic discrete interpolation scheme, so as to provide a so-called hybrid method [17]. In this case the choice of the optimal interpolation mesh for a required resolution must be determined by inspection, since for double spectral integrals it lacks the analysis analogous to the one given in [17] for single spectral integrals.

It is worthwhile to conclude by observing that linear analytic methods seem to provide the most suited computational instrument in the theoretical interpretation of experimental results of modern photoelectron spectroscopy, the trend being that of probing more and more detailed and local properties of electron eigenvalues and eigenstates. A simple example is offered by the study of angular dependence of photoelectric emission where by means of the linear analytic method [18] it is possible to overcome the computational inconveniences inherent to the naif root-sampling method.

Appendix

The initial-energy distribution of photoexcited electrons in the first interband transition of the nearly-free-electron model is analytically derived. The total density of state of the same model has been reported already [19].

The first two energy bands of the nearly-free-electron model [14] are

$$E_{1,2}(\mathbf{k}) = \tfrac{1}{2}[\mathbf{k}^2 + (\mathbf{k} - \mathbf{G})^2] \mp \tfrac{1}{2}\{[\mathbf{k}^2 - (\mathbf{k} - \mathbf{G})^2]^2 + 4V_{\mathbf{G}}^2\}^{1/2},$$

where **G** is the first reciprocal lattice vector in the k_x-direction, E_1 and E_2 refer to the valence and conduction bands, respectively, with the zero energy chosen so that $V_0 = 0$.

The distribution $N(E, \omega)$ of the initial energy of optically excited electrons arising from direct interband transitions is given by

$$N(E, \omega) = \frac{4V}{(2\pi)^3} \int d^3k F(\mathbf{k})\, \delta(\omega - E_2(\mathbf{k}) + E_1(\mathbf{k})) \times \delta(E - E_1(\mathbf{k}))$$

where V is the volume of crystal unit cell, ω is the photon energy, and $F(\mathbf{k})$ is the square dipole matrix element for the optical transition. By choosing as integration domain the right triangular prism $\{0 \leqslant k_x \leqslant \frac{1}{2}G, 0 \leqslant k_z \leqslant k_y \leqslant \frac{1}{2}G\}$ and by introducing the dimensionless variables $\mathbf{k}' = \mathbf{k}/\frac{1}{2}G$, $e = E/(\frac{1}{2}G)^2$, $w = \omega/(\frac{1}{2}G)^2$ and $n = N \cdot 2(\frac{1}{2}G)^4$ the integral becomes (omitting the prime)

$$n(e, w) = 16 \int_0^1 dk_x \int_0^1 dk_y \int_0^{k_y} dk_z\, F(\mathbf{k})\, \delta(w - e_2(\mathbf{k}) + e_1(\mathbf{k})) \times \delta(e - e_1(\mathbf{k})).$$

In what follows the integrand function is taken as constant since the derivation can be easily extended to the functions $F(\mathbf{k}) = k_y^m$ used in the numerical tests. If $F(\mathbf{k}) = 1$ then

$$n(e, w) = 16 \int_0^1 dk_x\, \delta(w - 4\{(1 - k_x)^2 + v^2/4\}^{1/2})\, K(e, k_x),$$

where $v = V_{\mathbf{G}}/(\frac{1}{2}G)^2$ and

$$K(e, k_x) = \int_0^1 dk_y\, J(e, k_x, k_y),$$

$$J(e, k_x, k_y) = \int_0^{k_y} dk_z\, \delta(e - f(k_x) - k_y^2 - k_z^2),$$

$$f(k_x) = 1 + (1 - k_x)^2 - 2\{(1 - k_x)^2 + v^2/4\}^{1/2}.$$

By means of the well-known properties of the Dirac delta function the integral J is easily obtained

$$J(e, k_x, k_y) = \frac{\theta(e - f(k_x) - k_y^2)\, \theta(k_y^2 - (e - f(k_x))/2)}{2\{e - f(k_x) - k_y^2\}^{1/2}},$$

θ being the unit-step function. In turn the function K is given by

$$K(e, k_x) = \frac{\pi}{8} \begin{cases} 0 & r \leqslant \frac{1}{2}, \\ \frac{4}{\pi} \sin^{-1} r^{1/2} & \frac{1}{2} \leqslant r \leqslant 1, \\ 1 & 1 \leqslant r, \end{cases}$$

where $r = r(e, k_x) = (e - f(k_x))^{-1}$. The last integration is trivial and provides the energy distribution

$$n(e, w) = 4\theta(w - 2v)\,\theta(4\{1 + v^2/4\}^{1/2} - w)\,K(e, 1 - ws/4)/s$$

where $s = \{1 - (2v/w)^2\}^{1/2}$.

Acknowledgment

The authors are grateful to R. Balossi for a careful reading of the Manuscript.

References

1. D. Brust, *Phys. Rev.* **139** (1965), A489.
2. R. Y. Koyama and N. V. Smith, *Phys. Rev. B* **2** (1970), 3049.
3. I. Petroff and C. R. Viswanathan, *Phys. Rev.* **4** (1971), 799.
4. N. W. Dalton and G. Gilat, *Solid State Commun.* **12** (1973), 211.
5. J. F. Janak, D. E. Eastman, and A. R. Williams, *Solid State Commun.* **8** (1970), 271.
6. J. F. Janak, *Solid State Commun.* **10** (1972), 833.
7. L. R. Saravia and L. Casamayou, *J. Phys. Chem. Solids* **32** (1971), 1075; **32** (1971), 1541; **33** (1972), 145.
8. L. J. Raubenheimer and G. Gilat, *Phys. Rev.* **157** (1967), 586.
9. G. Gilat and Z. Kam, *Phys. Rev. Lett.* **22** (1969), 715.
10. C. N. Berglund and W. E. Spicer, *Phys. Rev.* **136** (1964), A1030.
11. I. Abbati and L. Braicovich, *Riv. Nuovo Cimento* **4** (1974), 294.
12. E. O. Kane, *Phys. Rev.* **175** (1968), 1039.
13. L. van Hove, *Phys. Rev.* **89** (1953), 1189.
14. F. M. Mueller, J. W. Garland, M. H. Cohen, and K. H. Bennemann, *Ann. Phys. (N.Y.)* **67** (1971), 19.
15. G. Gilat and F. Herman, *Ann. Phys. (N.Y.)* **67** (1971), 432.
16. G. Ciucci and G. F. Nardelli, *in* "Proc. of the Twelfth International Conference on the Physics of Semiconductors" (M. H. Pilkuhn, Ed.), Teubner, Stuttgart, 1974.
17. G. Gilat, *J. Comp. Phys.* **10** (1972), 432.
18. R. Car, G. Ciucci, and L. Quartapelle, *Solid State Commun.* **21** (1977), 289.
19. N. W. Ashcroft, *in* "Computational Methods in Band Theory" (P. M. Marucs, J. F. Janak, and A. R. Williams, Eds.), Plenum, New York, 1971.